Structural, magnetic, and electronic properties of the Co-Fe-Al oxide spinel system: Density-functional theory calculations

Aron Walsh, Su-Huai Wei, Yanfa Yan, M. M. Al-Jassim, and John A. Turner
National Renewable Energy Laboratory, Golden, Colorado 80401, USA

Michael Woodhouse and B. A. Parkinson
Department of Chemistry, Colorado State University, Fort Collins, Colorado 80523, USA

(Received 3 July 2007; revised manuscript received 10 September 2007; published 18 October 2007)

A systematic study of nine binary and ternary spinel oxides formed from Co, Al, and Fe is presented by means of density functional theory. Analysis of the structural, magnetic, and electronic properties through the series of materials is carried out. Preference for the octahedral spinel sites are found in the order Fe < Co < Al. The electronic band gaps of Co_3O_4 and Fe_3O_4 are shown to remain largely unchanged as Al is substituted into the lattice forming M_2AlO_4 (M=Fe,Co), but increase greater than 1 eV for MAl_2O_4 as the octahedral M metal sites are lost. However, for stoichiometric $FeAl_2O_4$, the unsatisfied valence state of Fe results in partial occupation of the conduction band. The results and chemical trends are discussed in terms of atomic site and orbital energies, and in relation to potential photoelectrolysis activity for the splitting of water as a renewable means of hydrogen production.

DOI: 10.1103/PhysRevB.76.165119 PACS number(s): 81.05.Je, 61.50.Ah, 71.20.−b, 71.15.Mb

I. INTRODUCTION

Transition metal oxide-based photoelectrochemical (PEC) splitting of water has attracted extensive interest since photo-induced decomposition of water on TiO_2 electrodes was discovered.[1–4] However, thus far, no metal oxides have demonstrated promising and sustained efficiency. It is still necessary to search for new lower band gap materials that can potentially absorb visible light and exhibit reasonable PEC properties. Recently, Woodhouse *et al.*[5] have reported very interesting behaviors for the Co-Fe-Al oxide spinel system. With reported optical band gaps of between 1.1 (Ref. 6) and 1.65 eV (Ref. 7) for Co_3O_4 and 0.14 eV for low-temperature Fe_3O_4,[8] these two binary oxides have limited application in the PEC splitting of water. On introducing Al, the Co-Fe-Al oxide spinel system can exhibit optical band gaps of between 1.6 and 2.0 eV and generate a strong *p*-type photocurrent, which is ideal for PEC applications. In addition, other interesting behavior is found. For example, when the experiment is repeated without the Fe precursor, the photocurrent in the sample is reduced threefold, indicating that Fe does have an important role to play. X-ray diffraction revealed that the lattice constants of the synthesized materials are very similar within a large compositional range, which is very close to that of Co_3O_4. Unfortunately, although it is thought that the active material is Co and Al rich, further insight is restricted by the limited amount of information available about the properties of these spinels.

With a view to providing a better basic understanding of these Co, Al, and Fe containing oxides, we have calculated the electronic structure of nine stoichiometric spinels in both the normal and inverse structures, including the hypothetical Al_3O_4 compound. Calculations are performed using gradient corrected density functional theory with the Co and Fe 3*d* states treated with on-site correction for Coulomb interactions (DFT+U). The results can be summarized as follows: (i) The trends in the calculated lattice constants agree well with available x-ray diffraction data. The lattice constants increase along $Co_{3-n}Al_nO_4$ (n=0–3) and $Co_{3-n}Fe_nO_4$ (n=0–3), but decrease along $Fe_{3-n}Al_nO_4$ (n=0–3). (ii) Preference for the octahedral sites are found in the order Fe < Co < Al. (iii) The electronic band gaps of Co_3O_4 and Fe_3O_4 are shown to remain largely unchanged as Al is substituted into the lattice forming M_2AlO_4 (M=Fe,Co), but increase greater than 1 eV for MAl_2O_4 as the M octahedral sites are fully replaced. (iv) From the Co-Fe-Al spinel oxides studied, $CoAl_2O_4$ has been preliminarily identified as having the properties most suitable for PEC catalysis.

II. SPINEL STRUCTURE

The majority of ternary oxides of the form AB_2O_4 adopt the spinel structure as shown in Fig. 1. These materials, many of which are natural minerals, exhibit an interesting range of chemical properties largely derived from the wide range of cation distribution found in the spinel structure.[9–19] The cubic spinel crystal lattice, with space group $Fd\bar{3}m$, is based on a face centered cubic (fcc) packing of oxygen atoms. The A atoms, generally in a +2 oxidation state, occupy $\frac{1}{8}$ of the tetrahedral holes, while the B atoms, generally +3, occupy $\frac{1}{2}$ the available octahedral holes. In addition to this "normal" spinel arrangement, it is also possible for the B atoms to occupy tetrahedral sites with a mixture of A and B atoms distributed on the octahedral sites, conventionally referred to as the "inverse" spinel structure. Due to the ability of transition metals to adopt multiple oxidation states, binary oxides formed from these metals can also adopt the spinel structure, as demonstrated by both Co_3O_4 and Fe_3O_4. Co_3O_4 has recently received interest due to its catalytic activity in the decomposition of both N_2O and CH_4,[20,21] as well as its gas sensing properties.[22,23] Fe_3O_4 has been widely studied due to its ubiquitous magnetic properties[24] with growing interest in biomedical applications.[25,26]

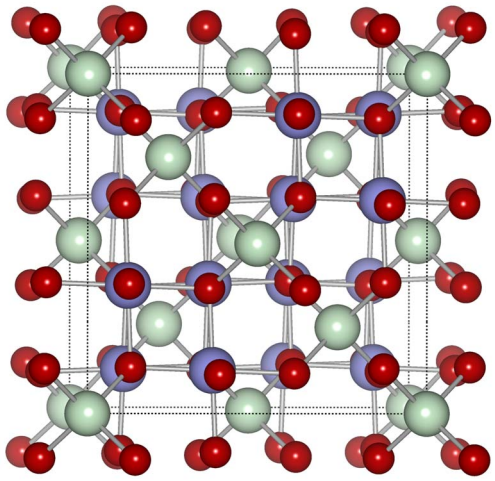

FIG. 1. (Color online) Illustration of the cubic AB_2O_4 spinel structure. The *A* atoms, colored green (light grey) occupy tetrahedral sites and the *B* atoms, colored blue (grey) occupy octahedral sites within a fcc oxygen sublattice colored red (dark grey).

In addition to the binary oxides, the ternary oxides of Co and Fe also show a strong preference for the spinel structure. Six stoichiometric ternary oxide spinels based around Co, Fe, and Al have been synthesized (Co_2AlO_4, $CoAl_2O_4$, Fe_2AlO_4, $FeAl_2O_4$, Co_2FeO_4, Fe_2CoO_4). There are very few detailed reports of the electronic structure of these spinel materials. In-depth structural studies of cation distributions in $CoAl_2O_4$ (cobalt blue)[27] and $FeAl_2O_4$ (hercynite)[28] have been reported. Two studies have looked at Fe_2CoO_4 in relation to potential magnetic applications[29,30] and its semiconducting properties have also been explored.[31] No systematic study has examined the properties of these ternary oxide spinels.

III. COMPUTATIONAL METHODS

Calculations were performed using density functional theory[32,33] under periodic boundary conditions, as implemented in the VASP code.[34,35] A plane wave basis set with a 500 eV upper energy threshold was employed, with a $6\times6\times6$ *k*-point grid for the Brillouin zone integration. The projector augmented wave method[36,37] was used to represent the valence-core interactions (Co, Fe:[Ar]; Al:[Ne]; O:[He]). The 14 atom primitive spinel unit cell was employed both for the normal and inverse spinels. For the inverse structure, distribution of the atoms over the octahedral sites was performed within the special quasirandom structure (SQS) model,[38] which ensures that the most physically relevant atomic correlations tend toward random occupation. This approach has been shown to give good results for cation distribution in other metal oxide spinels.[11,12]

All calculations were performed spin polarized within the scalar relativistic approximation. In systems with a potentially ambiguous magnetic structure, multiple spin configurations were explored, staying within the constraints of the primitive unit cell. The configurations resulting in the lowest total energy are reported in the results. It should be noted that the electronic structure and charge ordering of Fe_3O_4 has long been a matter of debate. While spinel structured Fe_3O_4 is known to go through a metal-insulator phase transition at 120 K to a lower symmetry monoclinic structure (Verwey transition), we will not be dealing with this effect as it has been explored in detail elsewhere.[39–41]

To correctly account for the highly correlated 3*d* orbitals of Fe and Co, the calculations were performed at the DFT $+U$ level[42,43] using the PBE gradient corrected exchange-correlation functional.[44] While values of U from 2 to 5 eV all produced qualitatively similar results in terms of the converged electronic structure, $U=2$ eV for Co 3*d* and $U=3$ eV for Fe 3*d* were chosen as they resulted in band gaps in the same region as available experimental data. It should be emphasized that while altering the value of U does change the absolute value of the electronic band gap, the qualitative changes and trends observed between these spinel materials are independent of such a selection. For example, $U=2$ eV applied to Co_3O_4 produces a direct Γ-Γ band gap of 1.67 eV with an indirect Γ-X transition of 1.51 eV, while $U=2.5$ eV results in Γ-$\Gamma=1.99$ eV and Γ-$X=1.79$ eV. In terms of the energy difference between the normal and inverse spinel structures, changes of U within the 2–5 eV range produce a variation of less than 0.1 eV. As the Al 3*s* states are relatively high in energy, both the valence and conduction band extrema are dominated by the transition metal *d* states. As such, the chosen values of U were taken to be transferable as Al is introduced into the binary Co and Fe oxides.

IV. RESULTS

A. Structural trends

To take into consideration the effects of cation distribution, calculations were performed for each of the ternary oxides in both the normal and inverse spinel structures. For clarity in the presentation, compounds which favor the normal spinel structure are written AB_2O_4, while compounds favoring the inverse spinel structure are written B_2AO_4. The lattice parameters and ionic positions were fully optimized so that the forces remained within 5 meV/Å. The equilibrium cell volumes were each obtained from an energy-volume fit to the Murnaghan equation of state.[45] The calculated lattice constants, inversion energy (ΔE) and equilibrium inversion parameter (δ^{eq}) for each system are listed in Table I. The inversion parameter approximates the cation distribution at a finite temperature (here taken as 1200 K), and is calculated as in Ref. 12. Values of δ^{eq} from 0 to 1 indicate a change in site preference from a normal to inverse spinel. The equilibrium bond lengths in each of the structures are listed in Table II. For the hypothetical Al_3O_4 spinel, the Al-O bond lengths are longer on the tetrahedral sites, indicating that these sites are more Al(II)-like than the Al(III) octahedral sites. The following trends can be observed.

(i) An increase in lattice constant as Al is added to Co_3O_4. For Co_3O_4 the optimized lattice constant (8.11 Å) is within 0.5% of experiment.[46] Replacing the tetrahedral Co sites with the larger Al ions results in a substantial expansion of the lattice to 8.25 Å. However, this structure is energetically

TABLE I. Calculated normal (N) and inverse (I) spinel lattice constants, along with experimentally determined values. ΔE is the difference in energy (per AB_2O_4 formula unit) between the normal and inverse spinel structures, while δ^{eq} is the calculated equilibrium inversion parameter at $T=1200$ K. A positive ΔE indicates the normal spinel is more stable.

Material	a^{exp} (Å)	$A(N)$ (Å)	$A(I)$ (Å)	ΔE (eV)	δ^{eq}
Co_3O_4	8.08	8.11	8.11		
Co_2AlO_4	8.09	8.25	8.16	−0.93 (I)	1.00
$CoAl_2O_4$	8.10	8.19	8.26	+0.52 (N)	0.11
Fe_3O_4	8.40	8.49	8.49		
Fe_2AlO_4	8.27	8.39	8.42	−0.26 (I)	0.93
$FeAl_2O_4$	8.16	8.23	8.34	+0.40 (N)	0.18
Al_3O_4		8.24	8.24		
Co_2FeO_4	8.24	8.19	8.27	−0.37 (I)	0.97
Fe_2CoO_4	8.39	8.52	8.40	−0.20 (I)	0.90

unfavorable relative to the inverse spinel where Al is substituted onto half of the octahedral Co sites. The calculated lattice constant for the inverse structure (8.16 Å) is closer to that of Co_3O_4 and indeed in much better agreement with the reported lattice constant of 8.09 Å for Co_2AlO_4.[47] The Al atoms in $CoAl_2O_4$ again exhibit a strong preference for the octahedral sites and here the normal spinel structure is most stable with a lattice constant (8.19 Å) within 1.1% of x-ray diffraction data.[48] Smaller Co-O bond lengths are observed for the octahedral Co site, in agreement with the observation that a higher oxidation state should result in a contraction of the ionic radius.[49] The two exceptions are the energetically less stable normal Co_2AlO_4 and inverse $CoAl_2O_4$ structures where Al occupies the tetrahedral sites, forcing the octahedral Co ion into a lower oxidation state.

TABLE II. The equilibrium cation-anion interatomic distances (in Å) in each of the normal (N) and inverse (I) spinel structures. For each M-O bond, larger bond lengths correspond to lower oxidation states.

Material	Co^{tet}	Co^{oct}	Fe^{tet}	Fe^{oct}	Al^{tet}	Al^{oct}
Co_3O_4	1.94	1.93				
Co_2AlO_4 (N)		2.05			1.80	
Co_2AlO_4 (I)	1.98	1.96				1.94
$CoAl_2O_4$ (N)	1.98					1.94
$CoAl_2O_4$ (I)		2.05			1.82	1.98
Fe_3O_4			1.91	2.08		
Fe_2AlO_4 (N)				2.10	1.81	
Fe_2AlO_4 (I)			2.02	2.04		1.97
$FeAl_2O_4$ (N)			2.00			1.94
$FeAl_2O_4$ (I)				1.97	2.03	1.97
Al_3O_4					1.97	1.96
Co_2FeO_4 (N)		1.94	1.98			
Co_2FeO_4 (I)	1.96	1.94		2.01		
Fe_2CoO_4 (N)	1.97			2.06		
Fe_2CoO_4 (I)		1.98	2.00	2.04		

(ii) A decrease in lattice constant as Al is added to Fe_3O_4. For Fe_3O_4, the optimized lattice constant (8.49 Å) is in good agreement with experiment (8.40 Å).[50] A decrease in the order of 0.10 Å in the lattice constant is observed for Fe_2AlO_4 in both the calculations and available diffraction data.[14] Al again shows an energetic preference for the octahedral spinel sites. A similar decrease in the lattice constant is observed for $FeAl_2O_4$ (Ref. 51), where the normal spinel structure is most energetically favorable. In contrast to Co, for the Fe oxides the smaller Fe-O bond lengths are observed for the tetrahedral Fe ion, suggesting that this is the higher oxidation state Fe site. It should be noted that the stability of the less stable inverse spinel structure of $FeAl_2O_4$ is increased when the octahedral sites are allowed to distort due to its metallic character.

(iii) An increase in the lattice constant as Fe is added to Co_3O_4. The calculated lattice constants of inverse Co_2FeO_4 (8.27 Å) and Fe_2CoO_4 (8.40 Å) lie in the range between the binary Co and Fe spinels and are in close agreement with the experimentally determined values of 8.24 and 8.39 Å, respectively.[52] It is worth noting that Co_2FeO_4 was reported as being metastable in the study by Ferreira *et al.*,[52] forming only when heated above 1170 K and segregating into Co and Fe rich spinel phases when cooled.

(iv) Cation distribution. Al, being a trivalent cation, is expected to exhibit a strong preference for the octahedral sites in the spinel structure, and this is reflected in the calculated inversion energies. Co can exist as a divalent or trivalent ion, but Co(III) is expected to have a strong preference for the octahedral sites from crystal field considerations, due to the stability of the Co $3d^6$ configuration in an octahedral environment.[10] Fe, which also can be a divalent or trivalent cation, is known to have a preference for the tetrahedral sites.[14] Occupation of the octahedral sites in the order Fe $<$ Co $<$ Al would therefore be anticipated. This order is unambiguously reflected as Al is substituted into the Co and Fe binary oxides, with the calculated inversion parameters in qualitative agreement with values derived from recent x-ray diffraction data.[53]

Fe_2CoO_4 exhibits a preference for the inverse spinel structure which can be understood through the preferred occupation of Co(III) on the octahedral sites. Co_2FeO_4 also favors the inverse structure, which at first is counterintuitive. However, as will be discussed for the magnetic structure in the following section, Fe is unusual in the fact that Fe(II) ions favor the octahedral sites, while the Fe(III) ions can occupy either site. In this way, for Co_2FeO_4, $Co(II)_{tet}[Fe(III),Co(III)]_{oct}$ is the most favorable configuration for satisfying the site preferences of both Co and Fe simultaneously. Experimentally, the occupation of tetrahedral sites by Co in Co_2FeO_4 is determined to be in excess of 50% depending on preparatory conditions.[52] This is in agreement with the calculations which indicate that the inverse spinel is more favorable by 0.37 eV/formula unit, although our calculated inversion parameter of 0.97 is clearly overestimated. This discrepancy is likely due to the simple model used in deriving the equilibrium inversion parameter,[12] and the possibility that the experimental value is not at its equilibrium state. The difference in lattice constant between the normal and inverse spinels is inherently included in the total energy calculations.

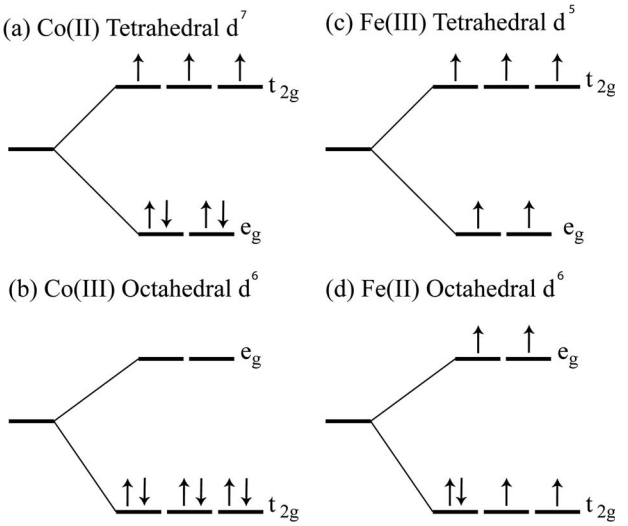

FIG. 2. Schematic crystal field splitting and occupations of the Co and Fe 3*d* electrons in tetrahadral and octahedral coordination environments.

TABLE III. Calculated magnetic moments (μ_B) for Co and Fe in each of the normal (*N*) and inverse (*I*) spinel materials.

Material	Co^{tet}	Co^{oct}	Fe^{tet}	Fe^{oct}
Co_3O_4	2.52	0.07		
Co_2AlO_4 (*N*)		2.81		
Co_2AlO_4 (*I*)	2.55	0.04		
$CoAl_2O_4$ (*N*)	2.57			
$CoAl_2O_4$ (*I*)		2.62		
Fe_3O_4			3.91	−3.94
Fe_2AlO_4 (*N*)				−3.94
Fe_2AlO_4 (*I*)			3.53	−4.07
$FeAl_2O_4$ (*N*)			3.61	
$FeAl_2O_4$ (*I*)				−3.59
Co_2FeO_4 (*N*)		−0.22	3.78	
Co_2FeO_4 (*I*)	2.47	0.09		−4.05
Fe_2CoO_4 (*N*)	2.45			−4.06
Fe_2CoO_4 (*I*)		0.13	3.51	−4.05

B. Magnetic structure

Although formal oxidation states overlook the mixture of ionic and covalent bonding which occurs in real crystals, they offer an intuitive starting point when considering the magnetic structure. Crystal field splittings and expected occupation of the 3*d* electrons of Co and Fe in their divalent and trivalent oxidation states are shown in Fig. 2. In Co_3O_4, the Co(II)/Co(III) ions are considered to occupy the tetrahedral and octahedral sites, respectively. However, for Fe_3O_4 an inverse occupation is the current viewpoint,[54] and is in agreement with our equilibrium bond lengths. The Fe(III) ions occupy the tetrahedral sites with an equal mixture of Fe(II)/(III) ions distributed on the octahedral sites, which are averaged to an effective oxidation state of +2.5.[29,30] In a tetrahedral crystal field, the e_g states are lowered in energy with respect to the t_{2g} states due to the electrostatic repulsion of the d_{zy}, d_{yz}, and d_{xz} orbitals, while in an octahedral environment the opposite is true and the d_{z2} and d_{x2-y2} orbitals are repelled. Experimental measurements of the magnetic moments support the fact that Co tends towards low spin configurations, while Fe favors high spin. This is demonstrated in Co_3O_4 where no magnetic moment is observed for the octahedral Co site, confirming a spin paired configuration,[55] Fig. 2(b), while Fe with a similar configuration exhibits a magnetic moment of $3.82\mu_B$,[56] Fig. 2(d). The calculated magnetic moments for the Co and Fe ions in each material are listed in Table III.

(i) Magnetic moment of Co. In each of the energetically stable structures, Co consistently favors a low spin configuration with no significant magnetic moment when placed on an octahedral site. However, when Al occupies the tetrahedral sites in the less stable normal Co_2AlO_4 and inverse $CoAl_2O_4$ structures, Co is forced into a d^7 configuration producing a magnetic moment of almost $3\mu_B$. This high spin configuration was also observed in a previous DFT study[27] of $CoAl_2O_4$ as the cation distribution was inversed. This observation is in agreement with the increase in Co-O bond length in the equilibrium structures. Small magnetic moments on the octahedral Co sites (up to $0.22\mu_B$) are also found when Fe occupies the tetrahedral site in normal Co_2FeO_4 and inverse Fe_2CoO_4. When placed on a tetrahedral site, Co exhibits a local moment around $2.5\mu_B$, with no exceptions.

(ii) Magnetic moment of Fe. Fe exhibits a moment of approximately $4\mu_B$ when placed on either a tetrahedral or octahedral site. While this is consistent with the occupations in an octahedral field shown in Fig. 2(d), it is substantially lower than the moment of $5\mu_B$ predicted in a tetrahedral field, Fig. 2(c). This discrepancy is due to the strong hybridization of unoccupied Fe 3*d* states with O 2*p* at the tetrahedral site.[56] While the moments of the tetrahedral ions in Fe_3O_4 are aligned, the moments between the tetrahedral and octahedral layers are most energetically favorable when in opposite phase. This antiferromagnetic alignment between layers also results in the most stable configuration when Co occupies the tetrahedral site and $\frac{1}{2}$ the octahedral sites in inverse Co_2FeO_4.

C. Electronic density of states

1. $Co_{3-n}Al_nO_4$ ($n=0-2$)

The total and projected electronic density of states (DOS) are shown for the most stable structures along the $Co_{3-n}Al_nO_4$ ($n=0,1,2$) series in Fig. 3.

(i) Co in a tetrahedral site. For the d^7 Co(II) ions in the tetrahedral sites, the majority spin *d* states are split between the e_g states at −6 eV and the t_{2g} states at −3 eV. The filled minority spin e_g states are situated at the top of the valence band, while the unoccupied minority t_{2g} states dominate the bottom of the conduction band at +2 eV. These conduction band states exhibit noticeable splitting for Co_3O_4 due to the coupling with Co at octahedral sites; this effect is reduced through the series.

(ii) Co in an octahedral site. The DOS derived for the octahedral Co(III) sites is almost symmetric with respect to

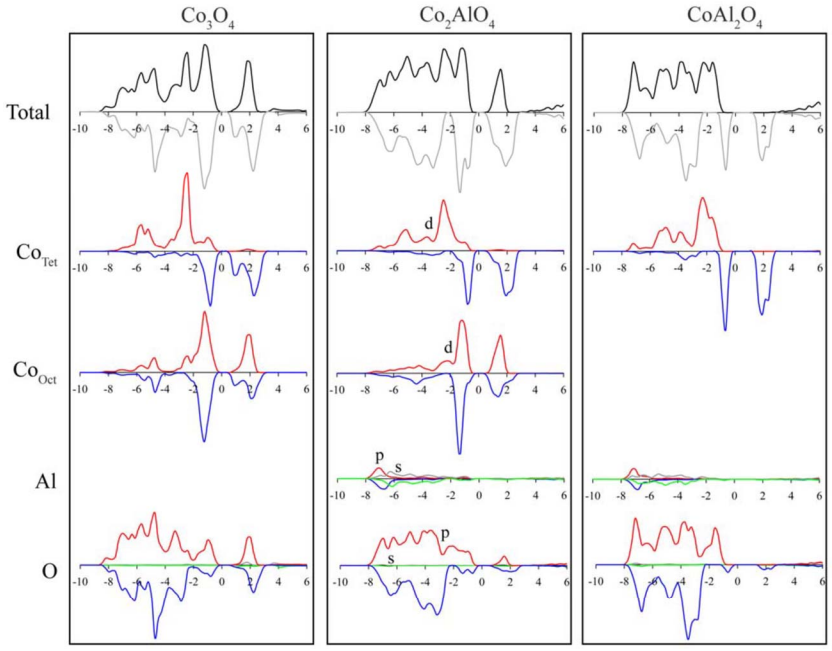

FIG. 3. (Color online) The electronic density of states of Co_3O_4, Co_2AlO_4 (inverse spinel), and $CoAl_2O_4$ (normal spinel), plotted with reference to the valence band maximum at 0 eV. For Co the red/blue lines represent ↑/↓ d states. For O and Al they represent ↑/↓ p states (magnified ×3), with the s states represented by grey/green.

the majority and minority spin states, in agreement with crystal field and magnetic moment expectations, Fig. 2(b). The Co $3d$ t_{2g} states are concentrated at the top of the valence band, about −1 eV, while some hybridize through oxygen with the tetrahedral Co $3d$ states at −5 eV. The e_g conduction band states are centered at +2 eV. The minority conduction band states exhibit a split indicative of coupling with the tetrahedral Co conduction band states in Co_3O_4 which is weaker for Co_2AlO_4. No octahedral Co sites are present in normal $CoAl_2O_4$.

(iii) Oxygen. The O $2p$ valence band runs from −8 to 0 eV. For Co_3O_4, coupling between the octahedral Co $3d$ states with O $2p$ results in a significant amount of oxygen p based conduction band states at +2 eV. As Al is introduced to the system, these states are diminished significantly with only a trace amount present in $CoAl_2O_4$.

2. $Fe_{3-n}Al_nO_4$ ($n=0-2$)

The DOS for the stable $Fe_{3-n}Al_nO_4$ ($x=0-2$) structures are shown in Fig. 4.

(i) Fe in a tetrahedral site. The d^5 tetrahedral Fe(III) ions adopt a high spin configuration with the majority spin t_{2g} and e_g states fully occupied, spread between −8 and 0 eV for both Fe_3O_4 and Fe_2AlO_4. The minority $3d$ states are situated in the conduction band. This is consistent with the occupations shown in Fig. 2(c). However, for $FeAl_2O_4$, Al(III) ions occupy the octahedral sites and Fe is forced into a +2 d^6

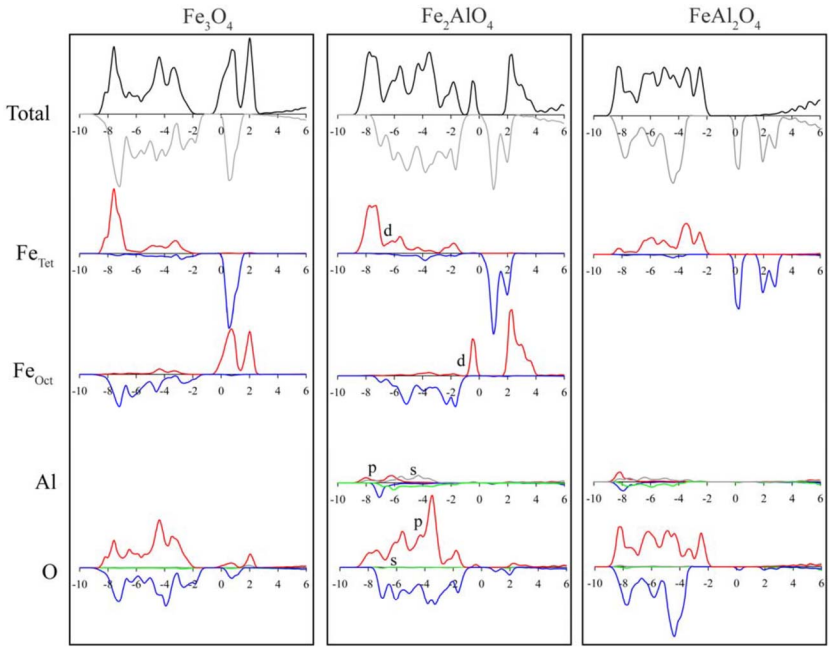

FIG. 4. (Color online) The electronic density of states of Fe_3O_4, Fe_2AlO_4 (inverse spinel), and $FeAl_2O_4$ (normal spinel), plotted with reference to the highest occupied state at 0 eV. For Fe the red/blue lines represent ↑/↓ d states. For O and Al they represent spin ↑/↓ p states (magnified ×3), with the s states represented by grey/green.

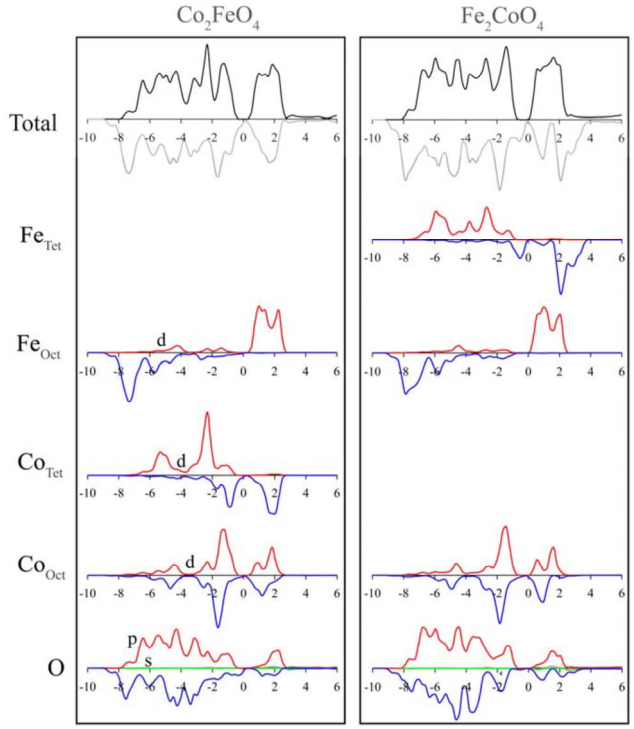

FIG. 5. (Color online) The electronic density of states of inverse Co_2FeO_4 and Fe_2CoO_4 plotted with reference to the highest occupied state at 0 eV. For Fe and Co the red/blue lines represent ↑/↓ *d* states. For O they represent spin ↑/↓ *p* states (magnified ×3), with the O *s* states represented by grey/green.

configuration, with partial occupation of the minority 3*d* conduction band state.

(ii) Fe in an octahedral site. For Fe_3O_4, the minority *d* states of the octahedral Fe sites are fully occupied, centered at approximately −7 eV. Due to the Fe d^6 electronic configuration, the majority t_{2g} states are partially filled, resulting in occupation of the conduction band which is the source of the semimetallic behavior in the cubic Fe_3O_4 spinel. As Al is introduced, electrons are added to the Fe t_{2g} bands and the enhanced Coulomb *U* splits the t_{2g} state, moving the occupied states closer to the valence band. The resulting decrease in the Fermi level results in a small finite band gap for Fe_2AlO_4 (not immediately visible in the DOS plot due to broadening in the integration of the bands). No octahedral Fe sites are present in normal $FeAl_2O_4$.

(iii) Oxygen. The O 2*p* contribution to the DOS is spread between −8 and 0 eV, similar to the Co based oxides. For Fe_3O_4, the coupling of O 2*p* with Fe 3*d* results in the presence of O 2*p*-based conduction band states at 2 eV, similar to, but weaker than Co_3O_4. As Al is introduced to the system, these states are again diminished significantly.

3. Co_2FeO_4 and Fe_2CoO_4

The DOS for Co_2FeO_4 and Fe_2CoO_4 in the more stable inverse spinel structure are shown in Fig. 5.

(i) Co_2FeO_4. The distribution of cation *d* states on each site roughly match the features observed in the previous spinels. However, here the octahedral Fe sites exhibit the characteristics of a high spin d^5 configuration (as opposed to d^6 in Fe_3O_4) with fully occupied majority *d* states and unoccupied minority states. Hybridization of the octahedral Co 3*d* states with oxygen results in the presence of O 2*p* states at the bottom of the conduction band, as observed in Co_3O_4. Coupling between the octahedral Co and Fe 3*d* states is indicated by a splitting of the majority spin conduction band states at +1.5 eV.

(ii) Fe_2CoO_4. In contrast to each of the previous Fe spinels studied, here the Fe(II) type ion occupies the tetrahedral site. While the majority spin states are fully occupied for both the Fe tetrahedral and octahedral sites, it is in the tetrahedral position that a single minority state is occupied at the top of the valence band, indicating that this site is closer to a d^6 configuration. The splitting of the octahedral Co and Fe conduction band states again indicates coupling between these states.

TABLE IV. The calculated direct Γ-Γ and *X*-*X*, and indirect Γ-*X* transitions (in eV) for both the normal (*N*) and inverse (*I*) Co-Al-Fe spinel structures.

Material	Γ-Γ (eV)	*X*-*X* (eV)	Γ-*X* (eV)
Co_3O_4	1.67	1.23	1.51
Co_2AlO_4 (*N*)	0.85	0.40	0.21
Co_2AlO_4 (*I*)	1.65	1.37	1.22
$CoAl_2O_4$ (*N*)	2.61	2.32	2.65
$CoAl_2O_4$ (*I*)	1.23	2.07	1.97
Fe_3O_4			
Fe_2AlO_4 (*N*)		0.51	
Fe_2AlO_4 (*I*)	0.44	0.85	0.99
$FeAl_2O_4$ (*N*)			
$FeAl_2O_4$ (*I*)			
Al_3O_4			
Co_2FeO_4 (*N*)	0.71	0.26	0.27
Co_2FeO_4 (*I*)	0.60	1.08	0.52
Fe_2CoO_4 (*N*)	0.45	0.75	0.53
Fe_2CoO_4 (*I*)	0.64	0.63	0.73

D. Electronic band gaps

In the calculated band structure of each system, Γ and *X* are the two high symmetry points which contribute to the valence and conduction band extrema. The lowest energy direct Γ-Γ and *X*-*X*, and indirect Γ-*X* electronic transitions are listed in Table IV. When placed in the spinel structure Al_3O_4 is calculated as being metallic; occupation of the conduction band is caused by the unsatisfied valence state of the tetrahedral Al ions.

1. $Co_{3-n}Al_nO_4$ ($n=0-2$)

For Co_3O_4 the valence band maximum (VBM) is a mixture of states derived from both tetrahedral Co 3*d* and O 2*p*, while the conduction band minima (CBM) is dominated by octahedral Co 3*d* states. Co_3O_4 has a calculated *X*-*X* transition energy of 1.23 eV, with an indirect Γ-*X* transition of

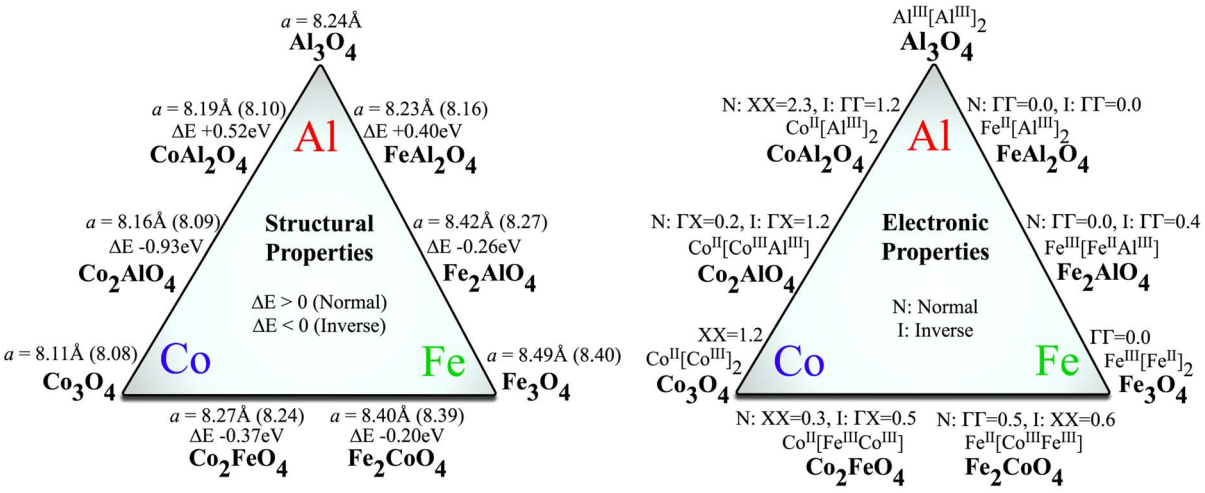

FIG. 6. (Color online) Summary of the calculated structural and electronic properties of the Co-Fe-Al oxide spinels. In the left panel, the experimental lattice constants are indicated in parentheses. In the right panel, the effective oxidation states of the cations in the most stable configuration are listed along with the lowest electronic transitions of both the normal (N) and inverse (I) structures.

1.51 eV and a direct transition at Γ of 1.67 eV. This is qualitatively in agreement with thin film optical measurements which observed a range of allowed and forbidden transitions from 1.1 to 2.06 eV.[6] For Co_2AlO_4, in the more stable inverse structure, there is a decrease in the direct gap at *X* and an increase in the Γ-*X* indirect gap, while the direct gap at Γ remains almost constant. The composition of the VBM and CBM are largely unchanged from Co_3O_4. However, for normal $CoAl_2O_4$ with no octahedral Co sites, each of the transition energies increase by more than 0.9 eV and the lowest energy transition of 2.32 eV is found at the *X* point. Here the VBM is still a mixture of tetrahedral Co 3*d* and O 2*p* states, while the CBM state is now almost entirely derived from tetrahedral Co 3*d* states. In this way, as the octahedral Co sites are lost, the band gap is increased. This is in good agreement with the UV-VIS absorbance onset of around 2 eV reported for bulk $CoAl_2O_4$.[57] For both Co_2AlO_4 and $CoAl_2O_4$, the less energetically stable spinel structures result in smaller electronic band gaps.

2. $Fe_{3-n}Al_nO_4$ ($n=0-2$)

Fe_3O_4 is calculated as being semimetallic in agreement with previous experimental and theoretical studies. However, when Al is introduced to the system a small bandgap opens up for the stable inverse Fe_2AlO_4 structure, while the top of the valence band is partially occupied for the normal spinel structure. For inverse Fe_2AlO_4, the lowest energy transition occurs at Γ (0.44 eV). For normal $FeAl_2O_4$ there is a large increase in each of the band gaps, with a Γ-Γ splitting of 2 eV. Similar to the cobalt spinels, this increase in band gap corresponds to a loss of octahedral Fe 3*d* sites. However, for normal $FeAl_2O_4$ due to presence of Al(III) on the octahedral sites, Fe is forced into a +2 d^6 configuration to preserve charge neutrality and there is occupation of the bottom of the conduction band. The less stable inverse structure of $FeAl_2O_4$ exhibits similar behavior.

3. Co_2FeO_4 *and* Fe_2CoO_4

To the best of our knowledge no experimental reports of the optical properties of either Co_2FeO_4 or Fe_2CoO_4 have been reported; however, conductivity measurements indicate an electronic gap in the region of 0.5–0.6 eV for stoichiometric Fe_2CoO_4.[31] The calculated lowest energy transition for inverse Co_2FeO_4 is indirect from Γ to *X* (0.52 eV), with a direct transition at Γ close in energy (0.60 eV). The calculated lowest energy gap of 0.63 eV in the inverse Fe_2CoO_4 spinel is in good agreement with electronic measurements and in reasonable agreement with the previously reported self interaction corrected DFT value of 0.8 eV.[30] The character of the VBM and CBM in both these materials contain a mixture of Co and Fe 3*d* states which result in the observed reduction in the electronic band gap from Co_3O_4.

V. DISCUSSION

The calculated structural and electronic properties of each oxide spinel studied, including the hypothetical Al_3O_4, are summarized in Fig. 6. The effective oxidation states in the stable structures, inferred from the equilibrium bonding lengths and calculated DOS are also shown. Co consistently favors a +2 d^7 configuration in a tetrahedral environment, with a +3 low spin d^6 configuration when placed in an octahedral environment. Fe always favors a high spin configuration, with +2 d^6 and +3 d^5 ions existing on both the tetrahedral and octahedral sites, depending on the electronic influence of the other cation constituents. Al shows little variation, with a strong preference for a +3 oxidation state on the octahedral sites.

While the Co and Fe 3*d* states have been shown to be active in determining the electronic and magnetic properties of these spinels, Al makes little contribution to the valence density of states. As such, when a ternary oxide is formed with majority Co and minority Al composition (Co_2AlO_4), Al occupies only half of the available octahedral sites, but it

is the remaining octahedral and tetrahedral Co sites that determine the properties. Hence, the electronic band gap is largely unchanged from Co_3O_4 to Co_2AlO_4. Increasing the Al composition of the ternary oxide to $CoAl_2O_4$ results in a loss of the octahedral Co sites, and as such, the band gap is increased as the octahedral Co 3*d* contribution to the CBM is no longer present. Conversely, Fe_3O_4 is semi-metallic due to the partial occupation of the conduction band. In Fe_2AlO_4, Al occupies half the octahedral sites breaking the Fe 3*d* coupling along the octahedral chain. This results in the opening of a small band gap for Fe_2AlO_4. For $FeAl_2O_4$ only the tetrahedral Fe sites remain and the band gap is largely increased, similar to $CoAl_2O_4$; however, the d^6 configuration of Fe on the tetrahedral sites results in partial occupation of the conduction band. The two ternary oxides formed from Co and Fe both result in small, but finite band gaps. Interestingly, considering the properties of the binary oxides, the Fe rich spinel Fe_2CoO_4 has a larger calculated band gap than the corresponding Co rich oxide Co_2FeO_4. In addition, experiment indicates that Co_2FeO_4 is not chemically stable at temperatures below 1170 K, while Fe_2CoO_4 is. Binding energies of Co_2FeO_4 and Fe_2CoO_4 calculated from the total energies of Co_3O_4 and Fe_3O_4 indicate that both these stoichiometric materials are energetically unstable; however, this may be a consequence of the small unit cells employed in our calculations which cannot fully account for the cation disorder which occurs in the real materials.

The qualitative trends of the calculated band gaps indicate that spinels formed from aluminum rich cobalt oxides would be best suited for application in a *p-n* photoelectrolysis system for hydrogen production from water. As noted in the introduction, Woodhouse *et al.*[5] identified a Co and Al rich spinel containing small amounts of Fe to be an active *p*-type material with an optical band gap of ~1.7 eV. Our results suggest that the band gap of ideal $CoAl_2O_4$ is too large to be directly considered, but Fe doping of this material or local cation disorder may reduce the band gap further, as the lower bandgap of the inverse spinel structure would suggest. Disorder is certainly a possibility in the reported photoelectrolysis material due to the low temperature (500 °C) synthesis conditions.[5] It is also possible for an active material to lie in the Co_3O_4 to Co_2AlO_4 range if doping or a high concentration of defects can make the fundamental gap larger and more direct. Future efforts should concentrate in detail on these regions and the effect of intrinsic defects, local cation disorder and Fe doping on the electronic structure and optical properties of these systems.

VI. CONCLUSION

In this study we have reported the electronic structure of three binary and six ternary Co, Fe, and Al containing oxide spinels. The trends in the calculated lattice constants agree well with the available experimental data. Preference for the octahedral spinel sites are found in the order Fe < Co < Al. The electronic band gap of Co_3O_4 is shown to remain largely unchanged as Al is substituted into the lattice forming Co_2AlO_4. Stoichiometric Fe_3O_4 is found to be semimetallic due to the partial occupation of the octahedral Fe 3*d* conduction band. For Fe_2AlO_4, the coupling between the octahedral Fe sites is broken, resulting in a finite band gap. For both $CoAl_2O_4$ and $FeAl_2O_4$, an increase in the band gaps of greater than 1 eV is observed as the octahedral sites are replaced by Al. However, the unsatisfied valence state of Fe in $FeAl_2O_4$ results in partial occupation of the conduction band. From the stoichiometric defect-free systems studied, $CoAl_2O_4$ has been preliminarily identified as having a direct electronic band gap close to the range suitable for photocatalytic activity in the splitting of water. However, future work is needed to assess the effects of intrinsic defects, extrinsic dopants, and local disorder on the electronic structure and resulting optical transitions of this system.

ACKNOWLEDGMENTS

This work was supported by the U.S. Department of Energy through the UNLV Foundation with Contract No. DE-AC36-99GO10337.

[1] A. Fujishima and K. Honda, Bull. Chem. Soc. Jpn. **44**, 1148 (1971).
[2] A. Fujishima and K. Honda, Nature (London) **238**, 37 (1972).
[3] A. Fujishima, K. Kohayakawa, and K. Honda, J. Electrochem. Soc. **122**, 1487 (1975).
[4] M. Gratzel, Nature (London) **414**, 338 (2001).
[5] M. Woodhouse, G. S. Herman, and B. A. Parkinson, Chem. Mater. **17**, 4318 (2005).
[6] P. S. Patil, L. D. Kadam, and C. D. Lokhande, Thin Solid Films **272**, 29 (1996).
[7] K. J. Kim and Y. R. Park, Solid State Commun. **127**, 25 (2003).
[8] S. K. Park, T. Ishikawa, and Y. Tokura, Phys. Rev. B **58**, 3717 (1998).
[9] A. Miller, J. Appl. Phys. **30**, S24 (1959).
[10] J. D. Dunitz and L. E. Orgel, J. Phys. Chem. Solids **3**, 318 (1957).
[11] D. Segev and S.-H. Wei, Phys. Rev. B **71**, 125129 (2005).
[12] S.-H. Wei and S. B. Zhang, Phys. Rev. B **63**, 045112 (2001).
[13] G. W. Watson and D. J. Willock, Chem. Commun. (Cambridge) **2001**, 1076.
[14] E. J. W. Verwey and E. L. Heilmann, J. Chem. Phys. **15**, 174 (1947).
[15] C. M. B. Henderson, J. M. Charnock, and D. A. Plant, J. Phys.: Condens. Matter **19**, 076214 (2007).
[16] E. Wolska, C. R. A. Catlow, P. Piszora, and S. M. Woodley, Comput. Chem. (Oxford) **24**, 603 (2000).
[17] M. J. Davies, S. C. Parker, and G. W. Watson, J. Mater. Chem. **4**, 813 (1994).
[18] J. S. Smart, Phys. Rev. **94**, 847 (1954).
[19] F. G. Brockman, Phys. Rev. **77**, 841 (1950).
[20] L. F. Liotta, G. Di Carlo, G. Pantaleo, and G. Deganello, Appl. Catal., B **70**, 314 (2007).

[21] C. Ohnishi, K. Asano, S. Iwamoto, K. Chikama, and M. Inoue, Catal. Today **120**, 145 (2007).
[22] H. J. Nam, T. Sasaki, and N. Koshizaki, J. Phys. Chem. B **110**, 23081 (2006).
[23] S. D. Choi and B. K. Min, Sens. Actuators B **77**, 330 (2001).
[24] A. R. Muxworthy and E. McClelland, Geochem. J. **140**, 101 (2000).
[25] S. J. Byrne, S. A. Corr, Y. K. Gun'ko, J. M. Kelly, D. F. Brougham, and S. Ghosh, Chem. Commun. (Cambridge) **2004**, 2560.
[26] S. A. Corr, Y. K. Gun'ko, A. P. Douvalis, M. Venkatesan, and R. D. Gunning, J. Mater. Chem. **14**, 944 (2004).
[27] F. Tielens, M. Calatayud, R. Franco, J. M. Recio, J. Perez-Ramirez, and C. Minot, J. Phys. Chem. B **110**, 988 (2006).
[28] M. Y. Lavrentiev, J. A. Purton, and N. L. Allan, Am. Mineral. **88**, 1522 (2003).
[29] V. N. Antonov, B. N. Harmon, and A. N. Yaresko, Phys. Rev. B **67**, 024417 (2003).
[30] Z. Szotek, W. M. Temmerman, D. Kodderitzsch, A. Svane, L. Petit, and H. Winter, Phys. Rev. B **74**, 174431 (2006).
[31] G. H. Jonker, J. Phys. Chem. Solids **9**, 165 (1959).
[32] P. Hohenberg and W. Kohn, Phys. Rev. **136**, B864 (1964).
[33] W. Kohn and L. J. Sham, Phys. Rev. **140**, A1133 (1965).
[34] G. Kresse and J. Furthmüller, Phys. Rev. B **54**, 11169 (1996).
[35] G. Kresse and J. Furthmüller, Comput. Mater. Sci. **6**, 15 (1996).
[36] G. Kresse and D. Joubert, Phys. Rev. B **59**, 1758 (1999).
[37] P. E. Blöchl, Phys. Rev. B **50**, 17953 (1994).
[38] S.-H. Wei, L. G. Ferreira, J. E. Bernard, and A. Zunger, Phys. Rev. B **42**, 9622 (1990).
[39] W. Friedrich, J. Phys.: Condens. Matter **14**, R285 (2002).
[40] H. P. Pinto and S. D. Elliott, J. Phys.: Condens. Matter **18**, 10427 (2006).
[41] H. T. Jeng, G. Y. Guo, and D. J. Huang, Phys. Rev. Lett. **93**, 156403 (2004).
[42] V. I. Anisimov, J. Zaanen, and O. K. Andersen, Phys. Rev. B **44**, 943 (1991).
[43] S. L. Dudarev, G. A. Botton, S. Y. Savrasov, C. J. Humphreys, and A. P. Sutton, Phys. Rev. B **57**, 1505 (1998).
[44] J. P. Perdew, K. Burke, and M. Ernzerhof, Phys. Rev. Lett. **77**, 3865 (1996).
[45] F. D. Murnaghan, Proc. Natl. Acad. Sci. U.S.A. **30**, 244 (1944).
[46] W. M. Shaheen and A. A. Ali, Mater. Res. Bull. **36**, 1703 (2001).
[47] P. G. Casado and I. Rasines, J. Solid State Chem. **52**, 187 (1984).
[48] H. S. C. O'Neill, M. James, W. A. Dollase, and S. A. T. Redfern, Eur. J. Mineral. **17**, 581 (2005).
[49] R. Shannon, Acta Crystallogr., Sect. A: Cryst. Phys., Diffr., Theor. Gen. Crystallogr. **32**, 751 (1976).
[50] C. Haavik, S. Stolen, H. Fjellvag, M. Hanfland, and D. Hausermann, Am. Mineral. **85**, 514 (2000).
[51] R. J. Hill, Am. Mineral. **69**, 937 (1984).
[52] T. A. S. Ferreira, J. C. Waerenborgh, M. H. R. M. Mendonca, M. R. Nunes, and F. M. Costa, Solid State Sci. **5**, 383 (2003).
[53] N. Tristan, J. Hemberger, A. Krimmel, H. A. Krug von Nidda, V. Tsurkan, and A. Loidl, Phys. Rev. B **72**, 174404 (2005).
[54] P. A. Cox, *The Electronic Structure and Chemistry of Solids* (Oxford University Press, New York, 1987).
[55] K. M. E. Miedzinska, B. R. Hollebone, and J. G. Cook, J. Phys. Chem. Solids **48**, 649 (1987).
[56] V. C. Rakhecha and N. S. Murthy, J. Phys. C **11**, 4389 (1978).
[57] U. Lavrenčič Štangar, B. Orel, and M. Krajnc, J. Sol-Gel Sci. Technol. **26**, 771 (2003).